

Forecasts for Helium Reionization Detection with Fast Radio Bursts in the Era of Square Kilometre Array

JUN-JIE WEI ^{1,2} AND CHONG-YU GAO^{1,2}

¹*Purple Mountain Observatory, Chinese Academy of Sciences, Nanjing 210023, China*

²*School of Astronomy and Space Sciences, University of Science and Technology of China, Hefei 230026, China*

ABSTRACT

The observed dispersion measures (DMs) of fast radio bursts (FRBs) are a good indicator of the amount of ionized material along the propagation paths. In this work, we present a forecast of He II reionization detection using the DM and redshift measurements of FRBs from the upcoming Square Kilometre Array (SKA). Assuming a model of the Universe in which He II reionization occurred at a specific redshift z_{re} , we analyze what extent the signal-to-noise ratio (S/N) for the detection of the amplitude of reionization can be achieved in the era of SKA. Using 10^6 mock FRB data from a one-year observation of the second phase of SKA, we find that the S/N for detecting He II reionization can approach the $32-50\sigma$ level and the uncertainty on the reionization redshift can be constrained to be $\sigma(z_{\text{re}}) \approx 0.022-0.031$, depending on the assumed FRB redshift distribution. This is the first quantitative analysis on the detection significance of He II reionization in the SKA era. We also examine the influence of different fiducial z_{re} values, finding that this effect has a modest impact on the forecasts. Our results demonstrate the potentially remarkable capability of SKA-era FRBs in constraining the epoch of He II reionization.

Keywords: Radio transient sources (2008) — Intergalactic medium (813) — Reionization (1383) — Observational cosmology (1146)

1. INTRODUCTION

Reionization is regarded as the latest phase transition in the Universe, transforming the baryonic gas from a neutral condition into an ionized state (Barkana & Loeb 2001). Understanding how and when the cosmic reionization happened is one of the important research topics in modern cosmology. Reionization usually refers to the process by which neutral hydrogen and helium atoms lost their first outer electrons at redshifts $z \gtrsim 6$ (e.g., Fan et al. 2002; Zaroubi 2013; Singh et al. 2018). During the epoch of hydrogen reionization, the high ionization potential (54.4 eV) of singly ionized helium (He II) kept its inner electron from being further ionized. The reionization of He II, caused by sufficient strong radiation from quasars and stars, is generally believed to occur at $z \sim 3$. The strongest evidence of He II reionization is obtained from observational signatures of the He II Ly α forest in the spectra of quasars at $z \sim 3$ (Syphers et al. 2009, 2012; Basu et al. 2024). Other evidence is the temperature change of the intergalactic medium (IGM; Furlanetto & Oh

2008a,b; McQuinn et al. 2009). The relatively lower redshift of He II reionization enables it more likely to be detected by next generation surveys.

Fast radio bursts (FRBs) are bright millisecond radio pulses predominantly originate at cosmological distances, the study of which is a hot spot in contemporary astrophysics (Lorimer et al. 2007; Cordes & Chatterjee 2019; Petroff et al. 2019, 2022; Xiao et al. 2021; Zhang 2023). Their all-sky rate is estimated to be as high as $\sim 10^4$ events day⁻¹ (Thornton et al. 2013). A direct observable of FRBs is the dispersion measure (DM) that encodes the integrated column density of ionized plasma along the line of sight. The observed DM is thus a good indicator of the amount of ionized baryons along the propagation path between the FRB source and the observer. Moreover, some FRBs with extremely high DM measurements are expected to be detected up to $z \gtrsim 6$ by future large-aperture telescopes (Fialkov & Loeb 2017; Zhang 2018; Hashimoto et al. 2020). Thanks to the short pulse nature, the high event rate, and the cosmological origin, FRBs are suitable for being used as a potentially new probe for the ionized IGM. Several studies have proposed that future DM measurements of high- z FRBs could be used to constrain the reionization history of hydrogen (e.g., Deng & Zhang 2014; Beniamini et al. 2021; Dai & Xia 2021; Hashimoto

et al. 2021; Pagano & Fronenberg 2021; Heimersheim et al. 2022; Maity 2024; Shaw et al. 2024) and helium (e.g., Deng & Zhang 2014; Zheng et al. 2014; Caleb et al. 2019; Linder 2020; Bhattacharya et al. 2021; Lau et al. 2021; Jing & Xia 2022). Since the current sample size and redshift range of localized FRBs are small, all such studies were performed by building mock FRB data sets.

As a next-generation radio astronomy-driven Big Data facility (Macquart et al. 2015), the Square Kilometre Array (SKA) will definitely have very powerful capability of detecting and localizing high- z FRBs (Fialkov & Loeb 2017; Hashimoto et al. 2020), which will offer a much larger population of FRBs for exploring the epoch of reionization. Therefore, it is natural to ask what level of reionization constraints can be achieved using future FRB data in the era of SKA. In view of the fact that He II reionization happened at a comparatively lower redshift and is more accessible to measurements, here we investigate the ability of the SKA-era FRB observation to detect He II reionization through Monte Carlo simulations.

But though FRBs have previously been proposed to constrain the epoch of He II reionization (Deng & Zhang 2014; Zheng et al. 2014; Caleb et al. 2019; Linder 2020; Bhattacharya et al. 2021; Lau et al. 2021; Jing & Xia 2022), it has not yet been quantitatively analyzed what extent the nature of He II reionization can be explored in the SKA era—our primary focus in this paper. Previously, Deng & Zhang (2014) and Zheng et al. (2014) first proposed the potential application of FRBs in probing He II reionization, Caleb et al. (2019) estimated the number of FRBs required to distinguish between a sudden He II reionization that occurred at $z = 3$ or 6 by using a two-sample Kolmogorov-Smirnov test, Linder (2020) assessed the ability of future high- z FRB samples to detect He II reionization, Bhattacharya et al. (2021) showed that the statistical ensemble of the DM distribution of FRBs prove useful probes of He II reionization even with limited redshift information, Lau et al. (2021) presented a cosmology-based model on determining the He II reionization redshift in range of $z = 3$ to 4 by detecting the DMs of distant FRBs, and Jing & Xia (2022) attempted to use the DM- z measurements of FRBs to derive the helium abundance in the Universe. In this work, we build on the techniques outlined by these authors by performing a forecast of the detection significance of He II reionization with the SKA-era FRB observation.

The rest of this paper is organized as follows. In Section 2, we show the imprint of the occurrence of He II reionization on the redshift function of the IGM portion of the DM, i.e., $DM_{\text{IGM}}(z)$, and describe the definition of a signal-to-noise ratio (S/N) for the detection of He II reionization. The expected detection rates of FRBs by SKA, the simulation method, and the relevant analysis results are presented in

Section 3. Finally, we give a brief summary and discussion in Section 4. Throughout this paper, we assume Λ CDM cosmology and adopt the cosmological parameters of $H_0 = 67.4$ km s $^{-1}$ Mpc $^{-1}$, $\Omega_m = 0.315$, $\Omega_b = 0.0493$, and $\Omega_\Lambda = 0.685$ (Planck Collaboration et al. 2020).

2. IMPACT OF HELIUM REIONIZATION ON DISPERSION MEASURE

For an extragalactic FRB propagating through the IGM, the cosmic DM in the observer frame is related to the free electron density (n_e) along the line of sight:

$$DM_{\text{IGM}}(z) = \int_0^z \frac{n_e(z')}{1+z'} dl'. \quad (1)$$

In a flat Λ CDM cosmology, the relation between proper length element dl' and redshift z' is given by

$$dl' = \frac{1}{1+z'} \frac{c}{H_0} \frac{dz'}{\sqrt{\Omega_m(1+z')^3 + \Omega_\Lambda}}, \quad (2)$$

where c is the speed of light, H_0 is the Hubble constant, Ω_m is the present-day matter density, and $\Omega_\Lambda = 1 - \Omega_m$ is the vacuum energy density. The number density of free electrons can be expressed as (Deng & Zhang 2014)

$$n_e(z) = \frac{\rho_{c,0} \Omega_b f_{\text{IGM}} X_e(z)}{m_p} (1+z)^3, \quad (3)$$

where $\rho_{c,0} \equiv 3H_0^2/8\pi G$ is the critical density of the Universe, m_p is the proton mass, Ω_b is the baryon density parameter, and $f_{\text{IGM}} \simeq 0.83$ is the mass fraction of baryons in the IGM (Fukugita et al. 1998). The electron fraction is

$$X_e(z) = Y_{\text{H}} X_{e,\text{HII}}(z) + \frac{1}{4} Y_{\text{He}} [X_{e,\text{HeII}}(z) + 2X_{e,\text{HeIII}}(z)], \quad (4)$$

where $Y_{\text{H}} = 1 - Y_{\text{He}}$ and Y_{He} are the hydrogen and helium abundances in the Universe, respectively, and $X_{e,\text{H}}(z)$ and $X_{e,\text{He}}(z)$ represent the ionization mass fractions of hydrogen and helium, respectively. The singly and doubly ionized elements are denoted by subscripts “II” and “III”, respectively. At a given redshift, the measured value of DM_{IGM} would vary along different lines of sight due to the large density fluctuations in IGM. In theory, the averaged DM_{IGM} over different lines of sight can be estimated by (Ioka 2003; Inoue 2004)

$$DM_{\text{IGM}}(z) = \frac{3cH_0\Omega_b f_{\text{IGM}}}{8\pi G m_p} \int_0^z \frac{(1+z')X_e(z')}{\sqrt{\Omega_m(1+z')^3 + \Omega_\Lambda}} dz'. \quad (5)$$

At the epoch of hydrogen reionization, both neutral hydrogen and helium are singly ionized by ionizing photons emitted from star-forming galaxies, $X_{e,\text{HeII}}$ can thus be approximated as $X_{e,\text{HII}}$ (e.g., Dai & Xia 2021). We suppose that hydrogen is fully ionized at $z = 6$ (i.e., $X_{e,\text{HII}} = 1$ and

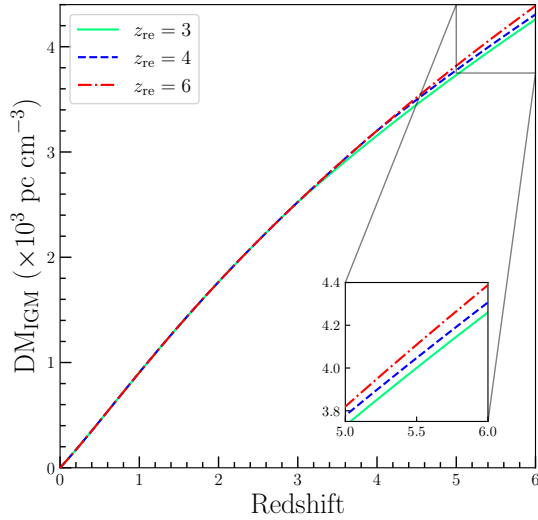


Figure 1. Sensitivity of the cosmic dispersion measure $DM_{\text{IGM}}(z)$ function to He II reionization. A sudden He II reionization is assumed to occur at redshift $z_{\text{re}} = 3, 4,$ and $6,$ respectively. The inset illustrates a zoomed-in view of the separation among different model curves.

$X_{e,\text{HeII}} = 1$) and that He II reionization occurs suddenly at redshift z_{re} (i.e., $X_{e,\text{HeII}} = 0$ and $X_{e,\text{HeIII}} = 1$). That is, considering the FRB sample up to redshifts $z < 6$, one has $X_{e,\text{HII}} = 1$, $X_{e,\text{HeII}} = 1$, and $X_{e,\text{HeIII}} = 0$ before He II reionization, while afterward $X_{e,\text{HII}} = 1$, $X_{e,\text{HeII}} = 0$, and $X_{e,\text{HeIII}} = 1$. Thus, $X_e(z > z_{\text{re}}) = 1 - 3Y_{\text{He}}/4 = 0.819$ and $X_e(z < z_{\text{re}}) = 1 - Y_{\text{He}}/2 = 0.880$, where we adopt the helium abundance inferred from Planck observations: $Y_{\text{He}} = 0.241$ (Planck Collaboration et al. 2020). The ionization fraction increases by $\sim 7.4\%$ because of He II reionization. That is, the sudden He II reionization would cause a change in DM_{IGM} (Equation 5).

It is interesting to explore whether we can detect such He II reionization in the $DM-z$ measurements of a high- z FRB sample. Following Linder (2020), we define a simple S/N criterion for the detection of He II reionization. In practice, we model the detection as (Linder 2020)

$$DM_{\text{IGM}}(z) = DM_{\text{IGM}}^{\text{high}}(z) + A_{\text{He}} \left[DM_{\text{IGM}}^{z_{\text{re}}}(z) - DM_{\text{IGM}}^{\text{high}}(z) \right], \quad (6)$$

where the superscripts “high” and “ z_{re} ” mean He II reionization occurs beyond the redshift limit of the sample and at $z = z_{\text{re}}$, respectively. If $A_{\text{He}} = 0$, then He II reionization is not detected by the sample, while $A_{\text{He}} = 1$ corresponds to reionization occurring at z_{re} . With $\sigma(A_{\text{He}})$ representing the uncertainty of the determined A_{He} , the detection S/N is thus $A_{\text{He}}/\sigma(A_{\text{He}})$, or simply $1/\sigma(A_{\text{He}})$ since it gives $A_{\text{He}} = 1$ if the modeling is right.

As an illustration, the DM of the IGM as a function of the redshift z is given in Figure 1. To show the effect of a sharp He II reionization on $DM_{\text{IGM}}(z)$, we plot three

cases with reionization occurring at $z_{\text{re}} = 3, 4,$ and $6,$ respectively. It is obvious that the cosmic DM has a change in slope at the reionization redshift due to the extra influx of electron fraction from He II reionization. The key questions are thus whether this signature (i.e., identify $A_{\text{He}} \neq 0$ with significant S/N) can be detected, and whether the redshift z_{re} at which reionization occurs can be measured. The model curves look pretty close together, as shown in Figure 1, but it should be underlined that the S/N for the detection of He II reionization would be enhanced by having enough high- z FRBs on either side of the reionization redshift. In the next section, we will investigate the prospect of He II reionization detection with the SKA-era FRB observation.

3. FORECASTING WITH FRB MOCK

3.1. Detection Rate of FRBs in the SKA era

Thanks to their extremely high event rate (Thornton et al. 2013), abundant FRBs are expected to be detected by the upcoming telescopes. Note that uncertainties in the fluence distribution and spectral index of the FRB population would make the estimate of the event detection rate for a specific telescope uncertain by several orders of magnitude (Vedantham et al. 2016; James et al. 2019; Zhang et al. 2023). However, it is feasible to give a simple calculation on the event detection rate at operating frequencies close to those at which FRB detections are conducted (i.e., 1.2–1.7 GHz, as probed by the SKA’s mid-frequency instrument), based on reasonable assumptions on the slope of the differential fluence distribution (i.e., the $\log N - \log F$ distribution). The cumulative all-sky event rate N_{sky} of FRBs above a given fluence threshold F_{ν} is generally described as a power-law model (Macquart & Ekers 2018),

$$N_{\text{sky}}(> F_{\nu}) = N'_{\text{sky}} \left(\frac{F_{\nu}}{F'_{\nu}} \right)^{\alpha}, \quad (7)$$

where N'_{sky} is the known event rate above the fluence threshold F'_{ν} estimated by existing FRB surveys, and the power-law index $\alpha = -1.5$ is in line with the expectation of a non-evolving population in Euclidean space (Vedantham et al. 2016).

The mid-frequency aperture array of the first phase of SKA (SKA1-MID) would reach a 10σ sensitivity of 14 mJy from 0.9 to 1.67 GHz for an integration time of 1 ms (Fender et al. 2015). While the actual scope of the second phase of SKA (SKA2) will eventually be subject to further discussions, the performance of SKA2 may be 10 times the SKA1 sensitivity in the frequency range of 0.35–24 GHz.¹ That is, the adopted 10σ fluence threshold of SKA2-MID is $F_{\nu} = 1.4$

¹ <https://www.skao.int/en/science-users/118/ska-telescope-specifications>

mJy ms. With Equation (7), we can estimate the all-sky event rate observed by SKA2-MID based on the rate measurements of Parkes and ASKAP telescopes. Bhandari et al. (2018) obtained $N'_{\text{sky}} = (1.7^{+1.5}_{-0.9}) \times 10^3 \text{ sky}^{-1} \text{ day}^{-1}$ above the fluence threshold of $F'_\nu = 2 \text{ Jy ms}$ from Parkes FRB surveys. Shannan et al. (2018) obtained $N'_{\text{sky}} = (37 \pm 8) \text{ sky}^{-1} \text{ day}^{-1}$ above the fluence threshold of $F'_\nu = 26 \text{ Jy ms}$ from ASKAP FRB surveys. Based on the Parkes result, the estimated all-sky event rate for SKA2-MID is

$$N_{\text{sky}} = (9.2^{+8.1}_{-4.9}) \times 10^7 \text{ sky}^{-1} \text{ day}^{-1}, \quad (8)$$

and according to the ASKAP result, we have

$$N_{\text{sky}} = (9.4 \pm 2.0) \times 10^7 \text{ sky}^{-1} \text{ day}^{-1}. \quad (9)$$

It is obvious that the two estimates are in good agreement with each other.

Considering the solid angle $\Delta\Omega$ covered on the sky by the SKA instantaneous observation, the expected number of FRBs can be estimated by

$$N_{\text{exp}} = \frac{\Delta\Omega}{4\pi} T N_{\text{sky}}, \quad (10)$$

where T is the exposure time on source. In general, the overall sky coverage of SKA2-MID would reach $\sim 25,000 - 30,000 \text{ deg}^2$ (Torchinsky et al. 2016). Since FRBs are transient phenomena, here we conservatively take $\Delta\Omega \approx 20 \text{ deg}^2$ ($\sim 0.006 \text{ sr}$) as the effective instantaneous field of view of SKA2-MID (Macquart et al. 2010). Following Zhang et al. (2023), we assume that SKA2-MID would spend an average of 20% of observing time per year on FRB search, and take $T = 20\% \times 365 \text{ day yr}^{-1}$. On the basis of the Parkes and ASKAP results, the expected detection rates of FRBs by SKA2-MID are then $\sim (3.3^{+2.9}_{-1.7}) \times 10^6 \text{ events yr}^{-1}$ and $\sim (3.3 \pm 0.7) \times 10^6 \text{ events yr}^{-1}$, respectively. Thus, we conclude that $\mathcal{O}(10^6)$ FRBs can be detected by SKA2-MID in a one-year observation.

The precise localization of FRBs is crucial for FRB cosmology. To obtain their host galaxy redshifts via optical follow-up, the positions of FRBs should be localized to within one arcsecond (Macquart et al. 2015). When complete, the SKA will have the ability of localizing FRBs to an accuracy of sub-arcseconds, and thus it is reasonable to expect that all the host galaxies of the SKA-detected FRBs would be identified and their redshifts would be measured.

3.2. Mock FRB Data

In this work, we perform Monte Carlo simulations to explore the prospect of He II reionization detection with future FRB measurements in the SKA era. The fiducial flat ΛCDM model with cosmological parameters derived from Planck observations ($H_0 = 67.4 \text{ km s}^{-1} \text{ Mpc}^{-1}$, $\Omega_m = 0.315$,

and $\Omega_b = 0.0493$; Planck Collaboration et al. 2020) is adopted to simulate FRB data. The fiducial values of the reionization parameters are taken to be $A_{\text{He}} = 1$ and $z_{\text{re}} = 3$, though we will discuss the effect of different fiducial z_{re} in the following subsection.

The redshift distribution of FRBs is expressed as

$$P(z) \propto \frac{4\pi D_C^2(z) c R(z)}{H(z)(1+z)}, \quad (11)$$

where $D_C(z) = c \int_0^z 1/H(z) dz$ is the comoving distance, $H(z)$ is the Hubble parameter, and $R(z)$ denotes the intrinsic event rate density distribution. So far, the actual $R(z)$ distribution of FRBs is poorly known. Qiang & Wei (2021) stressed that the assumed redshift distributions (i.e., the assumed $R(z)$ distributions) have significant effect on cosmological parameter estimation. The true redshift distribution of FRBs is inextricably linked to the corresponding progenitor system(s) of FRBs, and it is commonly assumed that the FRB rate follows the cosmic star formation history (SFH) or compact star mergers. In the merger model, a compact star binary system needs to experience a long inspiral phase before the final merger, so there is a significant time delay with respect to star formation. In the literature, three types of merger delay timescale models have been discussed (Virgili et al. 2011; Sun et al. 2015; Wanderman & Piran 2015): Gaussian delay model, lognormal delay model, and power-law delay model. Thus, we investigate four FRB event rate density models in detail:

- SFH model: we adopt the approximate analytical form derived by Yüksel et al. (2008) using a wide range of the star formation rate data

$$R(z) = \left[(1+z)^{3.4\eta} + \left(\frac{1+z}{5000} \right)^{-0.3\eta} + \left(\frac{1+z}{9} \right)^{-3.5\eta} \right]^{1/\eta}, \quad (12)$$

where $\eta = -10$.

- Compact star merger models: for the Gaussian delay model, we adopt the empirical formula (Virgili et al. 2011)

$$R(z) = \left[(1+z)^{5.0\eta} + \left(\frac{1+z}{0.17} \right)^{0.87\eta} + \left(\frac{1+z}{4.12} \right)^{-8.0\eta} + \left(\frac{1+z}{4.05} \right)^{-20.5\eta} \right]^{1/\eta}, \quad (13)$$

where $\eta = -2$.

- Compact star merger models: for the lognormal delay model (Wanderman & Piran 2015), the empirical for-

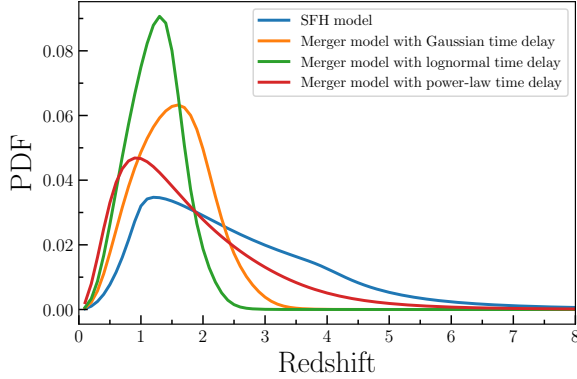


Figure 2. PDFs of redshifts derived from the SFH model and three compact star merger models with different merger delay time distributions (Gaussian, lognormal, and power-law).

mula of $R(z)$ is

$$R(z) = \left[(1+z)^{5.7\eta} + \left(\frac{1+z}{0.36}\right)^{1.3\eta} + \left(\frac{1+z}{3.3}\right)^{-9.5\eta} + \left(\frac{1+z}{3.3}\right)^{-24.5\eta} \right]^{1/\eta}, \quad (14)$$

where $\eta = -2$.

- Compact star merger models: for the power-law delay model (Wanderman & Piran 2015), one has

$$R(z) = \left[(1+z)^{1.9\eta} + \left(\frac{1+z}{2.5}\right)^{-1.2\eta} + \left(\frac{1+z}{3.8}\right)^{-4.4\eta} + \left(\frac{1+z}{7.7}\right)^{-11\eta} \right]^{1/\eta}, \quad (15)$$

where $\eta = -2.6$.

Figure 2 presents the FRB redshift distributions expected from all four assumed models. It is clear that the SFH model has the widest z distribution. Due to the merger delay, the other three merger models have narrower z distributions, with the overall redshift gradually shifting to lower redshifts in the order of power-law, Gaussian, and lognormal models (Zhang et al. 2021). Note that He II reionization is generally expected to occur at $z \sim 3$ (e.g., Becker et al. 2011). In order to effectively detect the signature of He II reionization, many high- z FRBs on either side of the expected reionization redshift are required. However, only low- z ($z \leq 3$) FRBs are predicted by the Gaussian and lognormal delay models (see Figure 2). For the rest of this paper, we shall therefore only consider two cases: the FRB redshift distribution tracing the SFH and power-law delay models, respectively.

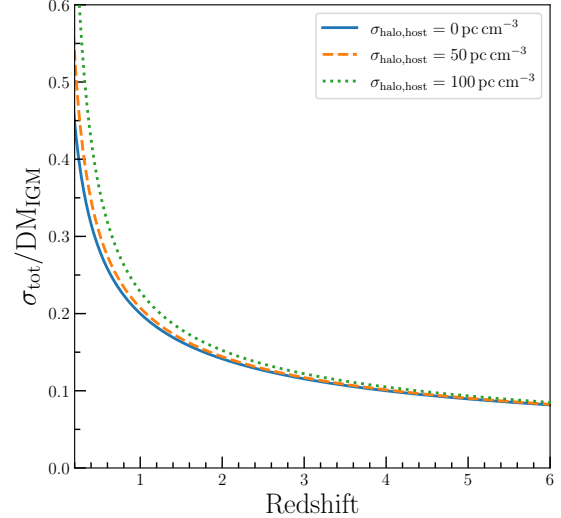


Figure 3. The fractional uncertainty on a measured DM_{IGM} , contributed by the IGM scatter (σ_{IGM}) and the uncertainty of the DM contributions from both the Milky Way halo and the FRB host galaxy ($\sigma_{\text{halo,host}}$), as a function of redshift. Curves show the quadrature sums of the two contributions for three cases with different $\sigma_{\text{halo,host}}$ values: 0 pc cm^{-3} (blue solid line), 50 pc cm^{-3} (yellow dashed line), and 100 pc cm^{-3} (green dotted line).

In our simulations, the true FRB host galaxy redshifts z^{true} are randomly generated from the probability density functions (PDFs) of Equation (11) for the SFH and power-law delay cases. After generating z^{true} , we simulate the measured redshifts z^{mea} by assuming an uncertainty of 10% on the spectroscopic data of host galaxies (as expected from the James Webb Space Telescope). That is, we draw z^{mea} from a Gaussian distribution $\mathcal{N}(\mu_z = z^{\text{true}}, \sigma_z = 0.1z^{\text{true}})$ (Heimersheim et al. 2022; Maity 2024).

With the true source redshift z^{true} , we infer the fiducial value of $DM_{\text{IGM}}^{\text{fid}}$ from Equation (6). Following previous works (Kumar & Linder 2019; Linder 2020), the line-of-sight fluctuation of DM_{IGM} (σ_{IGM}) is randomly added to the fiducial value of $DM_{\text{IGM}}^{\text{fid}}$, assuming

$$\sigma_{\text{IGM}} = 20\% \frac{DM_{\text{IGM}}^{\text{fid}}}{\sqrt{z^{\text{true}}}}. \quad (16)$$

That is, we sample the $DM_{\text{IGM}}^{\text{mea}}$ measurement according to the Gaussian distribution $DM_{\text{IGM}}^{\text{mea}} = \mathcal{N}(DM_{\text{IGM}}^{\text{fid}}, \sigma_{\text{IGM}})$. We note that the observed DM_{obs} has contributions from the interstellar medium (DM_{MW}) and dark matter halo (DM_{halo}) in the Milky Way, the IGM (DM_{IGM}), and the FRB host galaxy (DM_{host}). The DM_{IGM} value can then be derived by deducting DM_{MW} , DM_{halo} , and DM_{host} to DM_{obs} . While the corresponding uncertainty of DM_{IGM} should include the scatter due to the inhomogeneous IGM and the scatter caused by distinctive host properties and halo, the latter scatter (or-

der of 10 pc cm^{-3}) is much smaller than the former one (order of 10^2 pc cm^{-3}) at the reionization epoch (e.g., Prochaska & Zheng 2019). Figure 3 shows the evolution of the fractional uncertainty on a measured DM_{IGM} , accounting for the line-of-sight fluctuation of DM_{IGM} (σ_{IGM}) and the uncertainty of both DM_{halo} and DM_{host} ($\sigma_{\text{halo,host}}$), i.e., $\sigma_{\text{tot}} = (\sigma_{\text{IGM}}^2 + \sigma_{\text{halo,host}}^2)^{1/2}$. At low redshift, DM_{IGM} is small, so the fractional uncertainty $\sigma_{\text{tot}}/\text{DM}_{\text{IGM}}$ is relatively large. Since lines of sight average over IGM inhomogeneity and DM_{IGM} increases at higher redshift, $\sigma_{\text{tot}}/\text{DM}_{\text{IGM}}$ gradually decreases. Moreover, one can see from Figure 3 that adding the halo and host uncertainty (with the value of $\sigma_{\text{halo,host}} = 0, 50, \text{ or } 100 \text{ pc cm}^{-3}$) in quadrature gives negligible effect on $\sigma_{\text{tot}}/\text{DM}_{\text{IGM}}$, especially around the expected reionization redshift $z_{\text{re}} \gtrsim 3$. Therefore, we neglect the uncertainty of both DM_{halo} and DM_{host} subtractions from DM_{obs} to derive DM_{IGM} observationally.

Using the method described above, one can generate a catalog of the simulated FRB events with z^{mea} , $\text{DM}_{\text{IGM}}^{\text{mea}}$, and σ_{IGM} . Due to the lack of computational efficiency, we first simulate a population of 10^4 such events, assuming that the FRB redshift distribution follows the SFH model or the power-law delay model separately.

3.3. Results

For a set of 10^4 simulated FRBs, we only employ those FRBs with $z < 6$ for He II reionization parameter estimation, since the ionization fractions of hydrogen $X_{e,\text{HII}}(z)$ at $z \geq 6$ are not well understood and we take all of the hydrogen to be ionized at $z = 6$. We then utilize the standard Bayes theorem to explore the posterior probability distribution $\mathcal{P}(\theta|\mathcal{D})$ of the model parameters θ , provided the observed dataset \mathcal{D} , i.e.,

$$\mathcal{P}(\theta|\mathcal{D}) = \frac{\mathcal{L}(\mathcal{D}|\theta)\pi(\theta)}{\mathcal{P}(\mathcal{D})}, \quad (17)$$

where $\mathcal{L}(\mathcal{D}|\theta)$ is the likelihood of data conditional on the hypothetical model, $\pi(\theta)$ denotes some prior knowledge about the model parameters, and $\mathcal{P}(\mathcal{D})$ is the Bayesian evidence (which can be regarded as the normalized parameter and has no effect on our analysis). In our study, \mathcal{D} is the mock dataset consisting of $\text{DM}_{\text{IGM}}^{\text{mea}}$ and z^{mea} , and the free parameters to be constrained are $\theta = \{A_{\text{He}}, z_{\text{re}}\}$. The likelihood is given by (Maity 2024)

$$\begin{aligned} \mathcal{L}(\theta) = & \exp \left[-\frac{1}{2} \sum_i \left(\frac{\text{DM}_{\text{IGM},i}^{\text{mea}} - \text{DM}_{\text{IGM}}^{\text{th}}(z_i^{\text{true}}; \theta)}{\sigma_{\text{IGM},i}} \right)^2 \right] \\ & \times \exp \left[-\frac{1}{2} \sum_i \left(\frac{z_i^{\text{mea}} - z_i^{\text{true}}}{\sigma_{z,i}} \right)^2 \right], \end{aligned} \quad (18)$$

where $\text{DM}_{\text{IGM}}^{\text{th}}(z_i; \theta)$ is the theoretical value of DM_{IGM} calculated from the set of He II reionization parameters θ (see

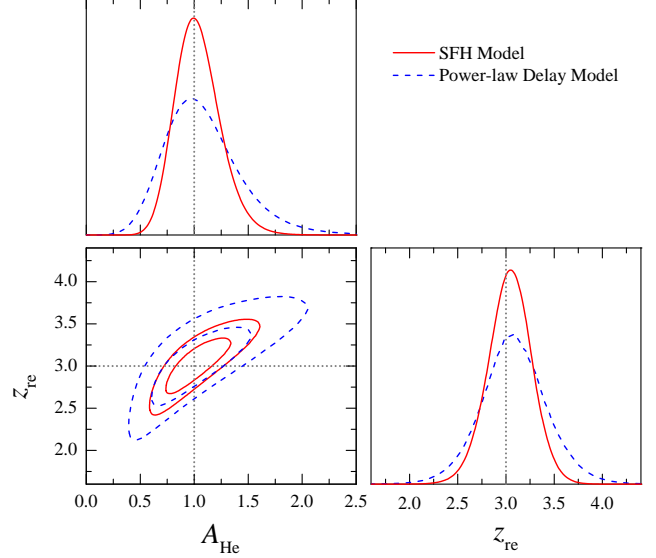


Figure 4. 1-D marginalized probability distributions and $1-2\sigma$ constraint contours for the reionization parameters A_{He} and z_{re} , using 10^4 simulated FRB events. The solid and dashed contours correspond to the cases of z distribution tracing the SFH model and the compact star merger model with power-law merger delay time distribution, respectively. The vertical dotted lines mark the input parameter values used to generate the FRB mocks.

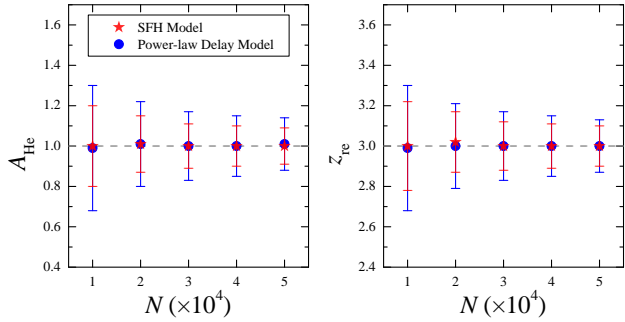
Equation 6). To ensure the final resulting constraints are unbiased, the simulation process is repeated 100 times for each FRB data set by using different noise seeds.

Figure 4 displays the resulting constraints on the reionization parameters A_{He} and z_{re} from 10^4 simulated FRBs. For the case of z distribution tracing the SFH model (solid contours), we find the marginalized parameter uncertainties $\sigma(A_{\text{He}}) = 0.20$ and $\sigma(z_{\text{re}}) = 0.22$. That is, the detection S/N for He II reionization is $\text{S/N} = A_{\text{He}}/\sigma(A_{\text{He}}) = 1.00/0.20 = 5.0$. Besides, the sudden reionization redshift can be inferred to be $z_{\text{re}} = 3.00 \pm 0.22$. To investigate the effect of z distribution, in Figure 4 we also plot those constraints obtained from the case of z distribution tracing the power-law delay model (dashed contours). Now we have $A_{\text{He}} = 0.99 \pm 0.31$ and $z_{\text{re}} = 2.99 \pm 0.31$. The detection S/N decreases to $\text{S/N} = A_{\text{He}}/\sigma(A_{\text{He}}) = 0.99/0.31 = 3.2$. We can see that the constraint precisions of A_{He} and z_{re} obtained from the power-law delay model are slightly worse than those from the SFH model. This is mainly because reionization parameters are more sensitive to high- z FRB data, and more high- z mock events, especially around the expected reionization redshift $z_{\text{re}} \gtrsim 3$, are generated in the SFH model (see Figure 2).

In order to comprehensively test what role the number of simulated FRBs (N) could play in He II reionization detection, we show the best-fit reionization parameters and their corresponding 1σ uncertainties as a function of N in Fig-

Table 1. Summary of Reionization Parameter Constraints from N Simulated FRB Events Using Different z Distributions

$N (\times 10^4)$	SFH Model		Power-law Delay Model	
	A_{He}	z_{re}	A_{He}	z_{re}
1	1.00 ± 0.20	3.00 ± 0.22	0.99 ± 0.31	2.99 ± 0.31
2	1.01 ± 0.14	3.02 ± 0.15	1.01 ± 0.21	3.00 ± 0.21
3	1.00 ± 0.11	3.00 ± 0.12	1.00 ± 0.17	3.00 ± 0.17
4	1.00 ± 0.10	3.00 ± 0.11	1.00 ± 0.15	3.00 ± 0.15
5	1.00 ± 0.09	3.00 ± 0.10	1.01 ± 0.13	3.00 ± 0.13

**Figure 5.** Best-fit reionization parameters (A_{He} and z_{re}) and their corresponding 1σ uncertainties as a function of the number of simulated FRB data. The star and circle symbols correspond to the cases of z distribution tracing the SFH and power-law delay models, respectively. The horizontal dashed lines stand for the fiducial values.

ure 5 and Table 1. We find that the uncertainties of these constraints from the FRB data are well consistent with the $1/\sqrt{N}$ behavior, independent of what kind of z distribution is assumed. According to our estimation of the FRB detection rate by SKA2-MID in Section 3.1, the one-year SKA2 observation would detect $\mathcal{O}(10^6)$ FRBs. In principle, it would be ideal to show the analysis with 10^6 mock FRBs. However, due to the lack of computational efficiency, we estimate the capacity of 10^6 mocks by extrapolating from present results of 10^4 mocks. Since all uncertainties will scale in proportion to the $1/\sqrt{N}$ behavior, 10^6 FRB data can give the reionization parameter uncertainties $\sigma(A_{\text{He}}) = 0.020$ and $\sigma(z_{\text{re}}) = 0.022$ ($\sigma(A_{\text{He}}) = 0.031$ and $\sigma(z_{\text{re}}) = 0.031$) for the case of z distribution tracing the SFH (power-law delay) model. Hence, for a one-year SKA2 observation with 10^6 FRBs, the detection S/N can approach 32–50.

In our above simulations, the fiducial reionization redshift is set to be $z_{\text{re}} = 3$. To study the effect of different fiducial z_{re} , we estimate the sensitivity as we vary z_{re} . Note that here we also mock a population of 10^4 FRBs with the z distribution following the SFH and power-law delay models, respectively. Figure 6 shows that no matter which z distribution is assumed, the S/N gets better rapidly with lower z_{re} , but falls below S/N = 1 for $z_{\text{re}} \gtrsim 4$. As the fiducial value of z_{re} grows, the reionization redshift uncertainty $\sigma(z_{\text{re}})$ becomes

larger. These are pretty easy to understand, because the number of FRBs at higher z_{re} is smaller (see the blue and red lines in Figure 2). Over the main range of the expected reionization redshifts, say $z_{\text{re}} \approx 2.5 - 3.5$, the S/N varies from 7.4 (5.0) to 3.2 (2.1), and $\sigma(z_{\text{re}})$ varies from 0.16 (0.21) to 0.29 (0.49) for the SFH (power-law delay) model.

In our analysis, we have neglected the uncertainty of the DM contributions from both the Milky Way halo and the FRB host ($\sigma_{\text{halo, host}}$), as described in Section 3.2. Although it seems to be a reasonable treatment as suggested by Figure 3, it would be good to add an analysis incorporating $\sigma_{\text{halo, host}}$ and check if there is any bias in the posterior recovery. Especially, when He II reionization is assumed to occur at $z = 2$, adding the halo and host uncertainty (for the maximum case of $\sigma_{\text{halo, host}} = 100 \text{ pc cm}^{-3}$) in quadrature gives a slight increase of $\sigma_{\text{tot}}/\text{DM}_{\text{IGM}}$ (see Figure 3). To investigate how sensitive our results on the uncertainties of A_{He} and z_{re} are on the choice of $\sigma_{\text{halo, host}}$, we also perform two parallel comparative analyses of 10^4 simulated FRBs using $\sigma_{\text{halo, host}} = 0 \text{ pc cm}^{-3}$ and 100 pc cm^{-3} , assuming that the fiducial reionization redshift is $z_{\text{re}} = 2$ and the z distribution traces the power-law delay model. If we change $\sigma_{\text{halo, host}}$ from 0 pc cm^{-3} to 100 pc cm^{-3} , then $\sigma(A_{\text{He}})$ goes from 0.135 to 0.144, and $\sigma(z_{\text{re}})$ from 0.145 to 0.154. So there is no concern regarding a possibly large dependence on $\sigma_{\text{halo, host}}$.

We emphasize that all our results are based on the assumption of sudden He II reionization. However, in reality, it is expected that the reionization phenomenon should evolve gradually with z . Assuming a linear evolution in redshift for the He II reionization within a range of $z_{\text{re, min}}$ to $z_{\text{re, max}}$, [Bhattacharya et al. \(2021\)](#) found that the difference between results for sudden reionization and gradual reionization is generally not significant. This is a positive outcome in the sense that our results on He II reionization detection are robust to the assumption about suddenness, but does imply that the duration of the reionization process is difficult to determine.

4. SUMMARY AND DISCUSSION

Cosmic reionization typically refers to the ionization of neutral hydrogen and helium at redshifts $z \gtrsim 6$. The singly ionized helium, He II, is expected to have undergone the same phase transition, but at a relatively lower redshift, and is often referred to as He II reionization. Compared to the

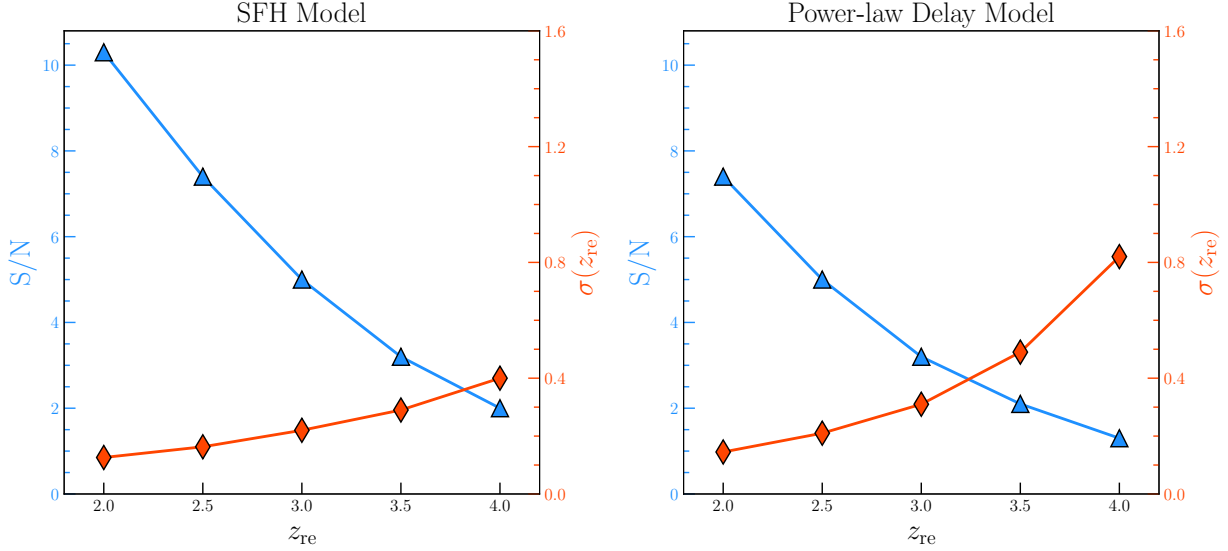


Figure 6. Sensitivity of the signal-to-noise ratio $S/N = A_{\text{He}}/\sigma(A_{\text{He}})$ for the detection of He II reionization and the uncertainty on the reionization redshift $\sigma(z_{\text{re}})$ to the fiducial value of z_{re} . All the constraints are derived from 10^4 simulated FRBs for the cases of z distribution following the SFH model (left panel) and the power-law delay model (right panel).

former one related to neutral hydrogen and helium reionization above $z \sim 6$, the later He II reionization is more accessible to observations by next generation surveys. FRBs, with their short pulse nature, high event rate, and large cosmological distance, are a promising tool for probing the epoch of He II reionization.

In this work, we have investigated the prospect of He II reionization detection with future FRB data to be detected by the upcoming SKA. With the definition of a simple S/N criterion for detecting He II reionization, we performed Monte Carlo simulations to assess the ability of the SKA-era FRB observation to constrain the detection S/N and the redshift z_{re} at which reionization occurs. In our simulations, we considered two different FRB redshift distributions: one is assumed to follow the SFH model, and the other one traces the compact star merger model with power-law merger delay time distribution. Based on a mock catalog of 10^4 FRBs, our results showed that the detection $S/N \approx 3.2 - 5.0$ and the uncertainty of the reionization redshift $\sigma(z_{\text{re}}) \approx 0.22 - 0.31$, depending on the assumed z distribution. Moreover, we confirmed that the uncertainties of the marginalized reionization parameters are in good agreement with the $1/\sqrt{N}$ behavior, with N the number of simulated FRBs. According to the existing FRB surveys and the possible detection performance of SKA2-MID, we expected that $\mathcal{O}(10^6)$ FRBs would be detected by SKA2 in a one-year observation. Since all the reionization parameter uncertainties will scale as $1/\sqrt{N}$, 10^6 FRB data can give $S/N \approx 32 - 50$ and $\sigma(z_{\text{re}}) \approx 0.022 - 0.031$. That is, for a one-year SKA2 observation with 10^6 FRBs, the S/N for the detection of He II reionization can approach the $32 - 50\sigma$ level. We also

inspected how the fiducial value of the reionization redshift z_{re} affect the forecasts for He II reionization detection, and found this effect was modest within the main range of the expected reionization redshifts.

It is worth highlighting that detecting high- z FRBs is very important scientifically. After the completion of SKA, an extensive dataset of high- z FRBs might become available. This would provide a great opportunity to utilize the DM measurements of high- z FRBs to directly probe the state of reionization in the IGM. Moreover, other world-leading radio survey telescopes such as the Hydrogen Intensity and Real-time Analysis eXperiment (HIRAX; [Newburgh et al. 2016](#)), Deep Synoptic Array 2000-dishes (DAS-2000; [Hallinan et al. 2019](#)), and Canadian Hydrogen Observatory and Radio-transient Detector (CHORD; [Vanderlinde et al. 2019](#)) are also anticipated to detect and localize tens of thousands of FRBs. With the rapid development of FRB detections, revealing the history of He II reionization with FRBs would be turned into reality.

1 We are grateful to the anonymous referee for construc-
 2 tive comments that have significantly improved our pre-
 3 sentation. This work is supported by the National SKA
 4 Program of China (2022SKA0130100), the National Nat-
 5 ural Science Foundation of China (grant Nos. 12422307,
 6 12373053, 12321003, and 12041306), the Key Research Pro-
 7 gram of Frontier Sciences (grant No. ZDBS-LY-7014) of
 8 Chinese Academy of Sciences, International Partnership Pro-
 9 gram of Chinese Academy of Sciences for Grand Challenges
 10 (114332KYSB20210018), the CAS Project for Young Sci-
 11 entists in Basic Research (grant No. YSBR-063), and the
 12 Natural Science Foundation of Jiangsu Province (grant No.
 13 BK20221562).

REFERENCES

- Barkana, R., & Loeb, A. 2001, *PhR*, 349, 125,
 doi: [10.1016/S0370-1573\(01\)00019-9](https://doi.org/10.1016/S0370-1573(01)00019-9)
- Basu, A., Garaldi, E., & Ciardi, B. 2024, *MNRAS*, 532, 841,
 doi: [10.1093/mnras/stae1488](https://doi.org/10.1093/mnras/stae1488)
- Becker, G. D., Bolton, J. S., Haehnelt, M. G., & Sargent, W. L. W. 2011, *MNRAS*, 410, 1096,
 doi: [10.1111/j.1365-2966.2010.17507.x](https://doi.org/10.1111/j.1365-2966.2010.17507.x)
- Beniamini, P., Kumar, P., Ma, X., & Quataert, E. 2021, *MNRAS*, 502, 5134, doi: [10.1093/mnras/stab309](https://doi.org/10.1093/mnras/stab309)
- Bhandari, S., Keane, E. F., Barr, E. D., et al. 2018, *MNRAS*, 475, 1427, doi: [10.1093/mnras/stx3074](https://doi.org/10.1093/mnras/stx3074)
- Bhattacharya, M., Kumar, P., & Linder, E. V. 2021, *PhRvD*, 103, 103526, doi: [10.1103/PhysRevD.103.103526](https://doi.org/10.1103/PhysRevD.103.103526)
- Caleb, M., Flynn, C., & Stappers, B. W. 2019, *MNRAS*, 485, 2281, doi: [10.1093/mnras/stz571](https://doi.org/10.1093/mnras/stz571)
- Cordes, J. M., & Chatterjee, S. 2019, *ARA&A*, 57, 417, doi: [10.1146/annurev-astro-091918-104501](https://doi.org/10.1146/annurev-astro-091918-104501)
- Dai, J.-P., & Xia, J.-Q. 2021, *JCAP*, 2021, 050, doi: [10.1088/1475-7516/2021/05/050](https://doi.org/10.1088/1475-7516/2021/05/050)
- Deng, W., & Zhang, B. 2014, *ApJ*, 783, L35, doi: [10.1088/2041-8205/783/2/L35](https://doi.org/10.1088/2041-8205/783/2/L35)
- Fan, X., Narayanan, V. K., Strauss, M. A., et al. 2002, *AJ*, 123, 1247, doi: [10.1086/339030](https://doi.org/10.1086/339030)
- Fender, R., Stewart, A., Macquart, J. P., et al. 2015, in *Advancing Astrophysics with the Square Kilometre Array (AASKA14)*, 51, doi: [10.22323/1.215.0051](https://doi.org/10.22323/1.215.0051)
- Fialkov, A., & Loeb, A. 2017, *ApJL*, 846, L27, doi: [10.3847/2041-8213/aa8905](https://doi.org/10.3847/2041-8213/aa8905)
- Fukugita, M., Hogan, C. J., & Peebles, P. J. E. 1998, *ApJ*, 503, 518, doi: [10.1086/306025](https://doi.org/10.1086/306025)
- Furlanetto, S. R., & Oh, S. P. 2008a, *ApJ*, 681, 1, doi: [10.1086/588546](https://doi.org/10.1086/588546)
- . 2008b, *ApJ*, 682, 14, doi: [10.1086/589613](https://doi.org/10.1086/589613)
- Hallinan, G., Ravi, V., Weinreb, S., et al. 2019, in *Bulletin of the American Astronomical Society*, Vol. 51, 255, doi: [10.48550/arXiv.1907.07648](https://doi.org/10.48550/arXiv.1907.07648)
- Hashimoto, T., Goto, T., On, A. Y. L., et al. 2020, *MNRAS*, 497, 4107, doi: [10.1093/mnras/staa2238](https://doi.org/10.1093/mnras/staa2238)
- Hashimoto, T., Goto, T., Lu, T.-Y., et al. 2021, *MNRAS*, 502, 2346, doi: [10.1093/mnras/stab186](https://doi.org/10.1093/mnras/stab186)
- Heimersheim, S., Sartorio, N. S., Fialkov, A., & Lorimer, D. R. 2022, *ApJ*, 933, 57, doi: [10.3847/1538-4357/ac70c9](https://doi.org/10.3847/1538-4357/ac70c9)
- Inoue, S. 2004, *MNRAS*, 348, 999, doi: [10.1111/j.1365-2966.2004.07359.x](https://doi.org/10.1111/j.1365-2966.2004.07359.x)
- Ioka, K. 2003, *ApJL*, 598, L79, doi: [10.1086/380598](https://doi.org/10.1086/380598)
- James, C. W., Ekers, R. D., Macquart, J. P., Bannister, K. W., & Shannon, R. M. 2019, *MNRAS*, 483, 1342, doi: [10.1093/mnras/sty3031](https://doi.org/10.1093/mnras/sty3031)
- Jing, L., & Xia, J.-Q. 2022, *Universe*, 8, 317, doi: [10.3390/universe8060317](https://doi.org/10.3390/universe8060317)
- Kumar, P., & Linder, E. V. 2019, *PhRvD*, 100, 083533, doi: [10.1103/PhysRevD.100.083533](https://doi.org/10.1103/PhysRevD.100.083533)
- Lau, A. W. K., Mitra, A., Shafiee, M., & Smoot, G. 2021, *NewA*, 89, 101627, doi: [10.1016/j.newast.2021.101627](https://doi.org/10.1016/j.newast.2021.101627)
- Linder, E. V. 2020, *PhRvD*, 101, 103019, doi: [10.1103/PhysRevD.101.103019](https://doi.org/10.1103/PhysRevD.101.103019)
- Lorimer, D. R., Bailes, M., McLaughlin, M. A., Narkevic, D. J., & Crawford, F. 2007, *Science*, 318, 777, doi: [10.1126/science.1147532](https://doi.org/10.1126/science.1147532)
- Macquart, J. P., & Ekers, R. 2018, *MNRAS*, 480, 4211, doi: [10.1093/mnras/sty2083](https://doi.org/10.1093/mnras/sty2083)
- Macquart, J.-P., Bailes, M., Bhat, N. D. R., et al. 2010, *PASA*, 27, 272, doi: [10.1071/AS09082](https://doi.org/10.1071/AS09082)
- Macquart, J. P., Keane, E., Grainge, K., et al. 2015, in *Advancing Astrophysics with the Square Kilometre Array (AASKA14)*, 55, doi: [10.22323/1.215.0055](https://doi.org/10.22323/1.215.0055)

- Maity, B. 2024, arXiv e-prints, arXiv:2408.05722, doi: [10.48550/arXiv.2408.05722](https://doi.org/10.48550/arXiv.2408.05722)
- McQuinn, M., Lidz, A., Zaldarriaga, M., et al. 2009, *ApJ*, 694, 842, doi: [10.1088/0004-637X/694/2/842](https://doi.org/10.1088/0004-637X/694/2/842)
- Newburgh, L. B., Bandura, K., Bucher, M. A., et al. 2016, in *Society of Photo-Optical Instrumentation Engineers (SPIE) Conference Series*, Vol. 9906, Ground-based and Airborne Telescopes VI, ed. H. J. Hall, R. Gilmozzi, & H. K. Marshall, 99065X, doi: [10.1117/12.2234286](https://doi.org/10.1117/12.2234286)
- Pagano, M., & Fronenberg, H. 2021, *MNRAS*, 505, 2195, doi: [10.1093/mnras/stab1438](https://doi.org/10.1093/mnras/stab1438)
- Petroff, E., Hessels, J. W. T., & Lorimer, D. R. 2019, *A&A Rv*, 27, 4, doi: [10.1007/s00159-019-0116-6](https://doi.org/10.1007/s00159-019-0116-6)
- . 2022, *A&A Rv*, 30, 2, doi: [10.1007/s00159-022-00139-w](https://doi.org/10.1007/s00159-022-00139-w)
- Planck Collaboration, et al. 2020, *A&A*, 641, A6, doi: [10.1051/0004-6361/201833910](https://doi.org/10.1051/0004-6361/201833910)
- Prochaska, J. X., & Zheng, Y. 2019, *MNRAS*, 485, 648, doi: [10.1093/mnras/stz261](https://doi.org/10.1093/mnras/stz261)
- Qiang, D.-C., & Wei, H. 2021, *PhRvD*, 103, 083536, doi: [10.1103/PhysRevD.103.083536](https://doi.org/10.1103/PhysRevD.103.083536)
- Shannon, R. M., Macquart, J. P., Bannister, K. W., et al. 2018, *Nature*, 562, 386, doi: [10.1038/s41586-018-0588-y](https://doi.org/10.1038/s41586-018-0588-y)
- Shaw, A. K., Ghara, R., Beniamini, P., Zaroubi, S., & Kumar, P. 2024, arXiv e-prints, arXiv:2409.03255, doi: [10.48550/arXiv.2409.03255](https://doi.org/10.48550/arXiv.2409.03255)
- Singh, S., Subrahmanyam, R., Udaya Shankar, N., et al. 2018, *ApJ*, 858, 54, doi: [10.3847/1538-4357/aabae1](https://doi.org/10.3847/1538-4357/aabae1)
- Sun, H., Zhang, B., & Li, Z. 2015, *ApJ*, 812, 33, doi: [10.1088/0004-637X/812/1/33](https://doi.org/10.1088/0004-637X/812/1/33)
- Syphers, D., Anderson, S. F., Zheng, W., et al. 2012, *AJ*, 143, 100, doi: [10.1088/0004-6256/143/4/100](https://doi.org/10.1088/0004-6256/143/4/100)
- . 2009, *ApJ*, 690, 1181, doi: [10.1088/0004-637X/690/2/1181](https://doi.org/10.1088/0004-637X/690/2/1181)
- Thornton, D., Stappers, B., Bailes, M., et al. 2013, *Science*, 341, 53, doi: [10.1126/science.1236789](https://doi.org/10.1126/science.1236789)
- Torchinsky, S. A., Broderick, J. W., Gunst, A., Faulkner, A. J., & van Cappellen, W. 2016, arXiv e-prints, arXiv:1610.00683, doi: [10.48550/arXiv.1610.00683](https://doi.org/10.48550/arXiv.1610.00683)
- Vanderlinde, K., Liu, A., Gaensler, B., et al. 2019, in *Canadian Long Range Plan for Astronomy and Astrophysics White Papers*, Vol. 2020, 28, doi: [10.5281/zenodo.3765414](https://doi.org/10.5281/zenodo.3765414)
- Vedantham, H. K., Ravi, V., Hallinan, G., & Shannon, R. M. 2016, *ApJ*, 830, 75, doi: [10.3847/0004-637X/830/2/75](https://doi.org/10.3847/0004-637X/830/2/75)
- Virgili, F. J., Zhang, B., O'Brien, P., & Troja, E. 2011, *ApJ*, 727, 109, doi: [10.1088/0004-637X/727/2/109](https://doi.org/10.1088/0004-637X/727/2/109)
- Wanderman, D., & Piran, T. 2015, *MNRAS*, 448, 3026, doi: [10.1093/mnras/stv123](https://doi.org/10.1093/mnras/stv123)
- Xiao, D., Wang, F., & Dai, Z. 2021, *Science China Physics, Mechanics, and Astronomy*, 64, 249501, doi: [10.1007/s11433-020-1661-7](https://doi.org/10.1007/s11433-020-1661-7)
- Yüksel, H., Kistler, M. D., Beacom, J. F., & Hopkins, A. M. 2008, *ApJL*, 683, L5, doi: [10.1086/591449](https://doi.org/10.1086/591449)
- Zaroubi, S. 2013, in *Astrophysics and Space Science Library*, Vol. 396, *The First Galaxies*, ed. T. Wiklind, B. Mobasher, & V. Bromm, 45, doi: [10.1007/978-3-642-32362-1_2](https://doi.org/10.1007/978-3-642-32362-1_2)
- Zhang, B. 2018, *ApJL*, 867, L21, doi: [10.3847/2041-8213/aae8e3](https://doi.org/10.3847/2041-8213/aae8e3)
- . 2023, *Reviews of Modern Physics*, 95, 035005, doi: [10.1103/RevModPhys.95.035005](https://doi.org/10.1103/RevModPhys.95.035005)
- Zhang, J.-G., Zhao, Z.-W., Li, Y., et al. 2023, *Science China Physics, Mechanics, and Astronomy*, 66, 120412, doi: [10.1007/s11433-023-2212-9](https://doi.org/10.1007/s11433-023-2212-9)
- Zhang, R. C., Zhang, B., Li, Y., & Lorimer, D. R. 2021, *MNRAS*, 501, 157, doi: [10.1093/mnras/staa3537](https://doi.org/10.1093/mnras/staa3537)
- Zheng, Z., Ofek, E. O., Kulkarni, S. R., Neill, J. D., & Juric, M. 2014, *ApJ*, 797, 71, doi: [10.1088/0004-637X/797/1/71](https://doi.org/10.1088/0004-637X/797/1/71)